mTORC2 Protects the Heart from Ischemic Damage

Mirko Völkers, Mathias H. Konstandin, Shirin Doroudgar, Haruhiro Toko, Pearl Quijada, Shabana Din, Anya Joyo, Luis Ornelas, Kaitlen Samse, Donna J. Thuerauf, Natalie Gude, Christopher C. Glembotski and Mark A. Sussman

Circulation. published online September 5, 2013;
Circulation is published by the American Heart Association, 7272 Greenville Avenue, Dallas, TX 75231

Print ISSN: 0009-7322. Online ISSN: 1524-4539

DOI: 10.1161/CIRCULATIONAHA.113.003638

mTORC2 Protects the Heart from Ischemic Damage

Running title: *Völkers et al.; Cardioprotection by mTORC2*

Mirko Völkers, MD; Mathias H. Konstandin, MD; Shirin Doroudgar, PhD; Haruhiro Toko, MD; Pearl Quijada, MS; Shabana Din, MS; Anya Joyo, BS; Luis Ornelas, BS; Kaitleen Samse, BS; Donna J. Thuerauf, MS; Natalie Gude, PhD; Christopher C. Glembotski, PhD; Mark A. Sussman PhD

SDSU Heart Institute, Department of Biology, San Diego State University, San Diego, CA

Address for Correspondence:
Mark A. Sussman, PhD
San Diego State University
Department of Biology
Life Sciences North, Room 426
5500 Campanile Drive, San Diego, CA, 92182, USA.
Tel: 619 594-2983
Fax: 619 594-8635
E-mail: heartman4ever@icloud.com

Journal Subject Codes: Basic science research:[130] Animal models of human disease, Basic science research:[131] Apoptosis, Myocardial biology:[108] Other myocardial biology

DOI: 10.1161/CIRCULATIONAHA.113.003638

Abstract

Background—The mechanistic target of rapamycin (mTOR) is comprised of two structurally distinct multiprotein complexes, mTOR complexes 1 and 2 (mTORC1 and 2). Deregulation of mTOR signaling occurs during and contributes to the severity of myocardial damage from ischemic heart disease. However, the relative roles of mTORC1 versus mTORC2 in the pathogenesis of ischemic damage are unknown.

Methods and Results—Combined pharmacological and molecular approaches were used to alter the balance of mTORC1 and mTORC2 signaling in cultured cardiac myocytes and in mouse hearts subjected to conditions that mimic ischemic heart disease. The importance of mTOR signaling in cardiac protection was demonstrated by pharmacological inhibition of both mTORC1 and mTORC2 with Torin1, which led to increased cardiomyocyte apoptosis and tissue damage after myocardial infarction (MI). Predominant mTORC1 signaling mediated by suppression of mTORC2 with Rictor similarly increased cardiomyocyte apoptosis and tissue damage after MI. In comparison, preferentially shifting toward mTORC2 signaling by inhibition of mTORC1 with PRAS40 led to decreased cardiomyocyte apoptosis and tissue damage after MI.

Conclusions—These results suggest that selectively increasing mTORC2 while concurrently inhibting of mTORC1 signaling is a novel therapeutic approach for the treatment of ischemic heart disease.

Key words: molecular biology, signal transduction, cardiac hypertrophy, cell signaling, cell death

DOI: 10.1161/CIRCULATIONAHA.113.003638

Ischemic damage impacts cardiac function through multiple mechanisms including infarction injury with cardiac myocyte death by apoptosis. The mechanistic target of rapamycin (mTOR), an atypical Ser/Thr protein kinase and central regulator of cell function, determines cell viability. mTOR signaling deregulation in cardiac disease contributes to cardiomyocyte apoptosis with associated impairment of cardiac function. mTOR resides in two distinct complexes, mTORC1 and mTORC2 [1,2]. Activation of mTORC1 phosphorylates several downstream targets including eukaryotic translation initiation factor 4E-binding protein (4E-BP) and ribosomal S6Kinase (S6K) that, in turn, phosphorylates ribosomal S6 protein (RibS6). In comparison, mTORC2 activation phosphorylates the pro-survival kinase Akt on Ser-473 required for Akt activation [3]. Although the mechanisms that regulate mTORC1 are well understood, regulation of mTORC2 is relatively poorly characterized.

mTOR signaling in cardiac physiology and disease has been examined by manipulating level and/or activity of mTOR kinase in hearts of mice. Conditional genetic deletion of mTOR kinase induced heart failure [4], whereas pharmacological inhibition of mTORC1 with rapamycin improved cardiac function in models of pressure overload, myocardial infarction, and hypertrophic cardiomyopathy [5-7]. Moreover, cardiomyocyte-specific mTOR overexpression protected hearts from challenge with pressure overload or ischemia [8,9]. Since mTOR kinase participates in signaling through mTORC1 and mTORC2, neither genetic nor pharmacological manipulation of mTOR kinase is sufficient to distinguish the roles of these two complexes in cardiac pathology. For example, while short-term inhibition of mTORC1 with rapamycin stimulates mTORC2 in cancer cells and in cardiac tissue [10,11], long term treatment with rapamycin decreases assembly and function of mTORC2 in cardiac tissue [10,12,13]. Moreover, rapamycin does not inhibit all mTORC1 functions [14]. In addition, pharmacological inhibition of

mTORC1 by rapamycin affects resident as well as infiltrating cells in the heart. Therefore, studies using systemic administration of rapamycin have been of limited value in delineating the relative importance of mTORC1 and mTORC2 in the heart. Thus, tissue- and cell-specific analyses of mTOR signaling are required to reveal the multifaceted role of mTOR.

Knockdown of Rictor, a component essential for mTORC2 function, decreases mTORC2 activity as well as Akt activation, and increased cell death with impaired proliferation in cancer cells [15,16]. Effects of mTOR2 inhibition in the non-cardiac context imply a role in the pathogenesis of ischemic heart disease, but cardiac-related studies of mTOR2 have not specifically addressed this issue. Therefore, acute myocardial infarction (MI) was used as the setting to assess the impact of mTORC2 signaling in amelioration of pathologic injury, with implications for mTORC2 as novel therapeutic target for cardiac ischemia.

Methods

Mice, Surgery, and Cardiac Function Analysis

Unless otherwise indicated, all experiments were performed in 7 week-old male C57BL/6 purchased from Jackson Laboratories. PI3Kgamma$^{-/-}$ mice and Akt1 KO$^{-/-}$ have been described previously [17]. Male mice underwent permanent ligation (myocardial infarction) of the left anterior descending coronary artery or a sham operation as previously described [18]. For echocardiography, mice were anesthetized with 2% isoflurane and scanned using a Vevo770 imaging system (Visual Sonics, ON, Canada), as previously described [19]. Closed chest hemodynamic assessment was performed after insertion of microtip pressure transducer (FT111B, Scisense) into the right carotid artery and advancement into left ventricle [19]. For *in vivo* injection of insulin, mice were injected i.p. with PBS or insulin (1U/kg/BW for 1h) after

overnight starvation. Institutional Animal Care and Use Committee approval was obtained for all animal studies.

Isolation and primary cultures of neonatal and adult ventricular cardiomyocytes

Isolation and primary cultures of neonatal and adult ventricular cardiomyocytes were prepared by standard procedures. Cells were treated with insulin (100nM) or H_2O_2 for multiple individual time points as indicated in figures.

Adenoviral constructs and siRNA

Recombinant adenoviruses were generated using human and mutated human PRAS40 cDNAs subcloned into the pShuttle-CMV vector using the AdEasy XL Adenoviral Vector system (Stratagene) as previously described[18]. The human full-length of PRAS40 contained a C-terminal FLAG tag. Neonatal rat cardiomyocytes and adult cardiomyocytes were infected with adenoviruses as described previously at a multiplicity of infection of 20 [20]

Adeno-Associated Virus Serotype 9 (AAV9) Generation and Systemic In Vivo AAV9 Cardiac-Targeted Gene Transfer Protocol

In vivo cardiac-targeted PRAS40 expression in normal mouse hearts was obtained by using tail vein injection of an adeno-associated virus serotype 9 (AAV9) harboring the PRAS40 gene or shRNA targeting Rictor (AAVshRictor) driven by a cardiomyocyte-specific CMV-MLC2v0.8 promoter or U6 promoter, respectively. Recombinant AAV9 vector carrying the same promoters without a downstream encoded transgene product served as control. 100 μL of 37°C heated Ringer Lactate containing 1×10^{11} total viral particles of either AAV9-control, AAV9-PRAS40 or AAV9 shRictor were injected into the tail vein, as previously described [21].

Sample preparation, immunoblotting, RT-qPCR

Whole hearts and isolated myocytes were prepared as described previously [18]. Immunoblots from

isolated cells or tissue were conducted as previously described. RNA was isolated using the Quick RNA MiniPrep kit (ZymoResearch) according the manufacturer's protocol. cDNA was generated and real-time quantitative PCR was carried out using the cDNA preparation kit and SYBR real-time PCR (Biorad) according to the manufacturer's protocol. Differences wee calculated using the ΔΔC(T) method. A full list of primers and antibodies is provided in the online supplement (**Supplemental Table 1-2**).

Histology and Staining

Immunostaining of isolated myocytes was performed on cells grown on Permanox chamber slides. Sections for Masson's trichrome, H&E, and immunohistochemistry were generated from paraffin-embedded hearts. Hearts were perfused *in situ* with formalin for 15 min, excised, and fixed in formalin for 24 hours at room temperature. Sections were deparaffinized using standard procedures. Immunostaining of paraffin-embedded hearts were performed, as described previously in detail [22]. Sections were also used to visualize the sarcolemma by staining with tetramethyl rhodamine isothiocyanate–conjugated wheat-germ agglutinin (Sigma-Aldrich). TUNEL staining was performed using the In Situ Cell Death Detection Kit, TMR red (Roche Applied Science) according to the manufacturer's directions.

Flow cytometry

Cell death was measured using an Annexin V kit (BD Biosciences), according to the manufacturer's instructions. To induce cell death, NRCMs were treated with 50μM H_2O_2 for 4h.

Statistical analysis.

Kaplan-Meier curves were generated to illustrate survival after myocardial infarction; statistical assessment was carried out by the log-rank test. Statistical analysis was performed using GraphPad Prism 5.0 (Graphpad Software Inc; www.graphpad.com). P values <0.05 were

considered significant. All the data sets were tested for normality of distribution using the Shapiro-Wilks test. To compare two groups with normal distribution Student's t-test was applied, otherwise a non-parametric test was used. Non parametric test were used when n<5 per group. For comparison of more than two groups 1-way ANOVA was applied, for the echocardiographic time course analysis repeated measure ANOVA was used, in both cases inclusive Bonferroni post hoc tests.

Results

mTOR activation after myocardial infarction

mTORC1 and mTORC2 signaling **(Figure 1A)** was assessed by phosphorylation of ribosomal S6 protein (RibS6; for mTORC1) and Akt (for mTORC2) following permanent occlusion of the left anterior descending (LAD) coronary artery at two days post-challenge. Phosphorylation of both proteins was increased in the infarcted mouse heart indicating activation of both mTORC1 and mTORC2 (**Supplemental Figure 1A)**. Activation of mTORC1 and mTORC2 in cardiomyocytes was confirmed by confocal immunolocalization of RibS6 and Akt^{S473} phosphorylation following infarction challenge **(Supplemental Figure 1A)**.

mTOR kinase inhibition with Torin1 increases cardiomyocyte death *in vitro*

Kinase activity of both mTORC 1 and 2 was inhibited using Torin1, a second- generation mTOR inhibitor **(Figure 1A)**. mTORC1 and mTORC2 were inhibited by Torin1 as shown by decreased insulin-dependent phosphorylation of S6K and Akt^{S473}, respectively, in a dose-dependent fashion whereas MAPK phosphorylation was unchanged (**Supplemental Figure 1B**). mTOR activity mediates survival in response to oxidative stress as demonstrated with Torin1 treatment (50 nM) of NRCM that blocks mTORC1 and mTORC2 activation in response to H_2O_2**(Figure 1B)**

consequently leading to increased cell death **(Figure 1C)**. The increased cell death after Torin1 treatment was mainly apoptotic as indicated by increased Annexin V binding (**Supplemental Figure 1C**)

mTOR kinase inhibition with Torin1 increases damage after MI

Acute mTOR inhibition *in vivo* was performed using Torin1 injected immediately after myocardial infarction (MI) with a short two-day follow up treatment to minimize systemic effects of the inhibitor. Pharmacokinetic properties of Torin1 render the compound short-lived [23]; therefore Torin1 was injected twice per day for two days (**Supplemental Figure 1D).** mTOR signaling assessment in mice receiving Torin1 treatment revealed decreased phosphorylation for downstream targets RibS6 and phosphorylation of Akt^{S473}, whereas Akt^{T308} phosphorylation was increased after MI (**Figure 1D**). Increased mortality was observed in Torin1-injected mice by 10 days after MI **(Figure 1E)** and infarct size was increased by 23% after Torin1 treatment compared to controls (**Figure 1F**). Apoptotic cell death contributed to increased infarct size and mortality following Torin1 administration as observed in myocardial sections where TUNEL labeling was significantly increased (**Figure 1G**). Ejection fraction was significantly impaired with a trend to enlarged left ventricular volume as a consequence of Torin1 treatment compared to control mice two weeks post MI, indicating that Torin1 treatment accelerated decompensation (**Figure 1H, Supplemental Table 3)**. Hemodynamic performance was also impaired in Torin1-treated animals relative to non-treated control MI groups (**Figure 1H)**. Heart rates were indistinguishable between the control and treated groups (**Supplemental Figure 1E**). Collectively, these findings indicate that inactivation of mTOR kinase activity is detrimental in the adaptive response to MI.

mTORC2 inhibition increases cardiomyocyte death *in vitro*

Functional activity for either mTORC1 or mTORC2 was selectively inhibited by targeted down-regulation of either Rictor or Raptor expression using siRNA (**see Figure 1A**) [1]. mTORC1 signaling was inhibited by siRNA-induced depletion of Raptor, without discernable effect upon mTORC2 activation, expression of Rictor **(Figure 2A-C)** or NRCM death **(Figure 2D).** mTOR protein levels were slightly reduced after knockdown of Raptor, consistent with prior observations in Raptor knockout mice (**Figure 2C**) [24]. mTORC2 signaling was inhibited by Rictor depletion using siRNA that was associated with increased cell death **(Figure 2D)** without apparent impact upon mTORC1 activation in response to H_2O_2 **(Figure 2E-G)**. Decreased NRCM survival was also observed by overexpression of Akt^{S473A}, a point mutant of the kinase that cannot be phosphorylated on Akt^{S473} **(Supplemental Figure 2A)**, showing that Akt^{S473} must be phosphorylated mTORC2 in order to mediate protection from oxidative stress. FoxO phosphorylation downstream of Akt was decreased after knockdown of Rictor whereas GSK3 phosphorylation remained unchanged (**Supplemental Figure 2B**), consistent with AKT^{S473} – mediated regulation of target molecules that influence cellular survival [25]. Increase in cell death after Rictor knockdown was primarily apoptotic as indicated by Annexin V positive cells consistent with the effect of Torin1 inhibition **(Supplemental Figure 2C)**.

mTORC2 inhibition increases damage after MI

mTORC2-selective inhibition by knocking down Rictor *in vivo* was accomplished using an shRNA targeted to mouse Rictor delivered via recombinant cardiotropic adeno-associated vector serotype 9 (AAV9). GFP-reporter virus was used to test the efficiency of the AAV9 mediated gene delivery. AAV9 mediated gene delivery resulted in 80% cardiomyocytes that are positive for the GFP-transgene measured by FACS **(Supplemental Figure 3A)**. Decreases in expression of Rictor (80% reduction) and mTORC2 signaling were confirmed in whole heart lysates two

days after infarction **(Figure 3A)** associated with diminished Akt^{S473} phosphorylation. Rictor knockdown did not affect either Raptor expression or mTORC1 activity compared to control mice, confirming specificity of decreased mTORC2 signaling **(Figure 3B-C)**, although total mTOR protein level was slightly decreased after Rictor knockdown (**Figure 3C**)**.** Increased mortality was associated with knockdown of Rictor during the first 10 after MI days **(Figure 3D)**, similar to the results obtained using Torin1 **(Figure 1D)**. Apoptotic cell death contributed to increased mortality, with TUNEL-positive cells increased following Rictor knockdown in myocardial sections (**Figure 3E**). Impaired systolic function with enlarged left ventricular chamber size was evident after Rictor knockdown compared to control animals **(Figure 3F, Supplemental Table 4).** Successful knockdown of Rictor in cardiomyocytes was confirmed by immunocytofluorescence (**Figure 3G**)**.** Increased fibrotic area resulted from knockdown of Rictor associated with pathological remodeling **(Figure 3H).** Therefore, mTORC2 inhibition decreases cardiomyocyte survival in response to MI challenge *in vivo*.

Decreased mTORC2 activity resulting from prolonged mTORC1 inhibition using rapamycin

Genetic deletion of Raptor inhibits mTORC1 signaling and increases mTORC2 function by suppressing a negative feedback loop, but also leads to severe cardiomyopathy [24]. Long-term pharmacological inhibition of mTORC1 with rapamycin was used to determine the impact upon TORC2 signaling. Indeed, mTORC2 signaling was disrupted after prolonged treatment of NRCM with rapamycin shown by diminished phosphorylation of the mTOR2 target Akt^{S473} **(Supplemental Figure 3B)**. Cell death inhibition after short-term treatment with rapamycin in response to H_2O_2 was abrogated upon long-term treatment **(Supplemental Figure 3B)**. Consequences of long-term inhibition of mTORC1 on mTORC2 signaling *in vivo* were assessed

by intraperitoneal injection of rapamycin daily for two weeks. mTORC2 signaling was unaffected by short-term treatment with rapamycin (2 mg/kg, first dose on the day of myocardial infarction) but prolonged treatment blocked Akt^{S473} after MI **(Supplemental Figure 3C)**. In conclusion, prolonged treatment with rapamycin also impairs mTORC2 function, similar to the effects of Torin1 in cardiomyocytes.

Increasing mTORC2 signaling while inhibiting mTORC1 decreases cardiomyocyte death

An endogenous molecular mechanism exists that blocks mTORC1 activity to regulate growth by maintaining the appropriate balance between anabolic processes and catabolic processes. PRAS40 (**P**roline **R**ich **A**kt **S**ubstrate of **40**kDa) is a specific component of mTORC1 that interacts with RAPTOR to inhibit mTORC1 kinase activity [26,27] has never been studied in the cardiac context. PRAS40 expression and regulation in myocytes was confirmed, with Akt-mediated phosphorylation of $PRAS40^{T246}$ that was absent in Akt1 KO mice **(Supplemental Figure 4A)**. Stimulation of Akt with insulin induced PRAS40 phosphorylation in isolated adult wild type myocytes **(Supplemental Figure 4B)**, thereby releasing the inhibitory function of PRAS40 on mTORC1 as previously described [26]. PRAS40-mediated inhibition of mTORC1 signaling after H_2O_2 stimulation was mediated by adenoviral overexpression of PRAS40 **(Supplemental Figure 4C)**. mTORC2 signaling was increased by PRAS40 expression as evidenced by higher levels of Akt^{S473} compared to controls after H_2O_2 stimulation (**Supplemental Figure 4D)**, consequently inhibiting apoptotic cell death **(Supplemental Figure 4E)**. Protective effects of PRAS40 against oxidative stress were abrogated by pharmacological inhibition of Akt or following overexpression a phosphorylation-impaired AktS473A that is point-mutated at a critical activation site of the kinase (Supplemental Fig. 4F). Increased PRAS40 phosphorylation is also observed in cardiomyocytes after MI **(Supplemental Figure**

5A-B). Thus, PRAS40 overexpression decreases mTORC1 and increases mTORC2 signaling, decreasing oxidative stress-induced cardiomyocyte death *in vitro*.

Loss of PRAS40-mediated cytoprotection upon inhibition of Akt prompted further studies to delineate involvement of mTORC2 using pharmacological and genetic approaches. Cytoprotective effects of PRAS40 were lost upon mTOR kinase inhibition using Torin1 (**Figure 4A**) that effectively inhibited both mTORC1 and mTORC2 (**Figure 4B**). Silencing of Akt expression increased cell death in NRCMs in all groups (**Figure 4C**) and PRAS40 was not protective when Akt is absent regardless of mTORC1 inhibition (**Figure 4D)**. mTORC2-mediated Akt activation was diminished after silencing of Rictor, abrogating the cytoprotective effect of PRAS40 overexpression. In contrast, silencing of Raptor expression that inhibits mTORC1 did not affect PRAS40-mediated protection (**Figure 4E**)**.** Efficiency of gene silencing in all studies involving either Raptor or Rictor, loss of mTORC1 function in Raptor deficient cells, or loss of mTORC2 in Rictor deficient cells was confirmed by immunoblots (**Figure 4F**). Protective effects of PRAS40 were not due to increased autophagy in our samples (data not shown). Taken together, these data show mTORC2 signaling is required for PRAS40-mediated protection and Akt activation is integral to cytoprotection in response to oxidative stress, *in vitro*.

Increasing mTORC2 signaling while inhibiting mTORC1 decreases damage after MI

Selective mTORC1 inhibition was achieved using PRAS40 delivered via recombinant cardiotropic adeno-associated vector serotype 9 (AAV9) with a cardiomyocyte-specific myosin light chain (MLC) promoter construct. (**Supplemental Figure 6A-B**). Strong transgene delivery of AAV9 MLC2 PRAS40 (80% positive cardiomyocytes) by tail vein injection was confirmed by counting of FLAG-tag positive cardiomyocytes (**Supplemental Figure 6 C**) similar to the results obtained with the GFP-reporter virus (**Supplemental Figure 3A**). PRAS40 expression

was increased approximately two-fold over endogenous levels in the heart three weeks after tail vein injection of AAV-PRAS40 without apparent change in cardiac function.

Increased mortality during the first 10 days post MI in in AAV-Control mice was significantly reduced by administration of AAV-PRAS40 (**Figure 5A**). Infarct size was reduced by 30% in AAV-PRAS40-treated mice compared to control mice (**Fig. 5B**), associated with decreased cell death in the infarct border zone (2.8% versus 1.6% TUNEL-positive cardiomyocytes in AAV-control and AAV-PRAS40, respectively; **Figure 5C**). AAV-PRAS40-treated mice showed significantly higher ejection fraction relative to the AAV-Control group within one week post infarction. End diastolic and end systolic dimensions were reduced in AAV-PRAS40 mice relative to the AAV-Control group, indicative of blunted remodeling with AAV-PRAS40 (**Figure 5D, Supplemental Table 5**) that was maintained over the 6 week time course for assessment. Hemodynamic performance was improved and end diastolic pressure was reduced in AAV-PRAS40 relative to AAV-Control mice at termination of the study six weeks after MI (**Figure 5E**). Heart rate was comparable between the groups (**Supplementary Fig. 6D**). Hypertrophic increase in the heart weight/Body weight ratio (HW/BW) was blocked in PRAS40-overexpressing mice (**Figure 5F**), consistent with blunted increases in cardiomyocyte cross-sectional area and hypertrophic gene signature in mice receiving AAV-PRAS40 relative to the AAV-Control group (**Figure 5G-H**). Decreased pathological remodeling resulted in less fibrosis in PRAS40 overexpressing mice measured by Mason-Trichrome Staining and Collagen1 transcription 6 weeks after MI **(Figure 5I-J).** Overall, PRAS40 selectively inhibited mTORC1 in cardiomyocytes, thereby protecting against MI damage and characteristic sequelae *in vivo.*

Mechanism of PRAS40 mediated protection

Molecular mechanisms of PRAS40-mediated reduction in ischemic injury were correlated with

assessments of mTOR signaling in the acute phase after MI. AKT^{S473} phosphorylation in AAV-PRAS40-treated hearts displayed a 9.7-fold increase of AKT^{S473} in the infarct zone together with increased PRAS40 phosphorylation relative to a 6.3-fold increase in AKT^{S473} phosphorylation for AAV-Control hearts at two days post-MI (**Figure 6A and Supplementary Figure 6E**). Akt^{T308} phosphorylation was also increased in AAV-PRAS40-treated hearts compared to AAV-Controls. As intended, mTORC1 activation was decreased by 39% by AAV-PRAS40 after MI, along with 5.7 fold higher RibS6 phosphorylation in AAV-control mice compared to sham operated animals (**Figure 6B).** Enhanced AKT^{S473} phosphorylation (**Figure 6C**) and reduced mTORC1 activation (**Figure 6D**) consequential to AAV-PRAS40 administration was confirmed by immunohistochemistry. AKT^{S473} phosphorylation increases persist in AAV-PRAS40 treated hearts up to six weeks after MI surgery (**Figure 6E-F**) without evidence of pathological hypertrophy (**Figure 5F**) or RibS6 phosphorylation in the border zone **(Supplementary Figure 6F)**. Preservation of insulin receptor substrate 1 (IRS-1) expression in hearts of the AAV-PRAS40 group relative to the AAV-Control group at six weeks (**Figure 6E**) suggests that decreased mTORC1 signaling slows degradation of IRS-1, consequently improving insulin signaling and mTORC2 function. Expression of the sarcoplasmic reticulum ATPase (SERCA2a) was decreased and sodium-calcium exchanger (NCX1) increased in AAV-Control hearts in the remote area 6 at six weeks, but remained essentially unchanged in AAV-PRAS40 treated hearts compared to sham operated animals (**Figure 6E and Supplemental Figure 6G**).

mTORC2 deletion diminishes PRAS40-mediated protection from infarction injury

Participation of the PI3K-mTORC2-Akt pathway in PRAS40-mediated cardioprotection *in vivo* was established using genetically engineered mouse strains lacking PI3K or AKT. Global deletion of $PI3K^{-/-}$ results in impaired Akt activation in response to MI [28]. $PI3K^{-/-}$ mice treated

with AAV-PRAS40 or AAV-Control show comparable cardiac function at eight weeks of age (**Figure 7A**), but cardioprotection conferred by AAV-PRAS40 was absent in PI3K$^{-/-}$ mice relative to wild-type control mice at 1 week after MI. AAV-PRAS40 also fails to provide protective effects in Akt1 null mice with comparable decline in cardiac function between AAV-Con or AAV-PRAS40 after MI (**Figure 7B**). Comparable PRAS40 overexpression between all groups of mice was confirmed by immunoblots (**Supplementary Figure 7A-B**). Causality of mTORC2 function for PRAS40-mediated cardioprotection was established using Rictor knockdown with AAV (AAV-sh-Rictor). Experimental groups consisted of mice receiving AAV-sh-Rictor alone or in conjunction with AAV-PRAS40 and control groups receiving AAV-sh-Control alone or in combination with AAV-PRAS40 injected at 7 weeks of age followed by MI three weeks later. AAV-sh-Rictor treatment exacerbated decline in cardiac function whereas AAV-PRAS40 improved ejection fraction measured two weeks after MI challenge (**Figure 7C**). Moreover, AAV-sh-Rictor decreased cardiac function and increased left ventricular dimension in mice receiving the otherwise cardioprotective AAV-PRAS40 treatment (**Figure 7C**). mTORC1 function was impaired in mice receiving AAV-PRAS40 as evidenced by blunted hypertrophic remodeling (**Figure 7D**). Apoptotic cell death increased with AAV-sh-Rictor treatment and decreased with AAV-PRAS40 treatment, but cytoprotection from AAV-PRAS40 was overridden by AAV-sh-Rictor (**Figure 7E**). In summary, mTORC2 activity is responsible for the protective effects of PRAS40 *in vivo* **(Figure 8)**.

Discussion

Loss of viable myocardium after myocardial infarction is the leading cause of cardiac dysfunction resulting in chronic heart failure. A cardioprotective role for mTORC2 activation in

cardiomyocytes following myocardial infarction is supported by findings presented in this study. Pharmacological inhibition with second-generation mTOR inhibitors and genetic silencing of Rictor results in increased ischemic damage and is associated with increased mortality after myocardial infarction, consistent with a beneficial role for mTORC2.

Role of mTORC2 signaling in ischemic damage

Surprisingly little is known about the specific role of mTORC2 in cell survival other than impairment of mTORC2 function by Rictor knockdown worsens cell survival *in vitro* [29]. Moreover, evidence for a direct role of mTORC2 in regulating survival after ischemic damage *in vivo* has never been reported to our knowledge. Genetic and pharmacologic evidence show that mTORC1 inhibition is beneficial after myocardial infarction [5-7,30-32]. However, feedback occurring mTORC1 and mTORC2 signaling upon rapamycin treatment intertwines the relative roles of these two distinct complexes and renders the system inadequate to dissect apart the specific role of mTORC2 in cell survival and disease progression.

Pharmacological inhibition of mTOR kinase function with Torin1 is detrimental to cardiomyoctes both *in vitro* and *in vivo* after myocardial infarction (**Figure 1**), consistent with genetic evidence that mTOR deletion results in lethal fully penetrant dilated cardiomyopathy [4] and highlighting the importance of intact mTOR signaling in cell survival and function. Moreover, use of novel mTOR kinase inhibitors to treat cancer may carry with them inherent cardiotoxic side effects in patients, especially those with co-morbidities of heart failure or infarction injury. With next generation mTOR inhibitors entering clinical trials it is imperative to further characterize their cardiotoxic potential [33].

Genetic deletion of mTORC2 is associated with increased ischemic damage (**Figure 3**). Findings presented here confirm the important role of mTORC2, Rictor, and Akt^{S473}

phosphorylation in cardiomyocytes to control cellular survival. Previous studies show Rictor plays a critical role in maintaining tissue metabolism, T-cell development, and neuronal function, but the role of Rictor in response to ischemic tissue injury has not been explored[15,34,35]. Silencing of Rictor exacerbates negative consequences after myocardial infarction (**Figure 3**), supporting the premise that Rictor plays an important role in regulation cellular survival after ischemic damage. Reduced Akt^{S473} phosphorylation after Rictor silencing cascades into decreased phosphorylation of downstream targets for Akt including FoxO that presumably could contribute to cell death [36,37]. Further confirmation of an essential role for Akt^{S473} phosphorylation was evident from use of a phosphorylation-deficient inactive Akt mutant (S473->A) unable to block cell death in response to oxidative stress (**Supplemental Figure 2**). Indeed, prior studies show that mTORC2 regulates Akt substrate specificity for downstream phosphorylation targets including FoxO, GSK3 and TSC2 [25]. Importantly, chronic use of rapamycin disrupts mTORC2 function in cardiomyocytes and compromises cell survival (**Supplemental Figure 3**). Detrimental side effects of chronic rapamycin administration in the clinical setting demonstrate a pressing need for studies to elucidate cardiotoxicity risk, especially in combination with ischemic injury.

PRAS40 is cardioprotective via increased mTORC2 signaling

Although short-term inhibition of mTORC1 with rapamycin is beneficial after myocardial infarction, long-term treatment disrupts mTORC2 function. Therefore approaches to block mTORC1 in myocytes using selective endogenous molecular inhibitors can provide beneficial effect of blocking pathologic responses without compromising cell survival. PRAS40 was initially identified as a 14-3-3 binding protein [38] and was subsequently found to be an mTORC1 inhibitor and substrate [26,27,39,40]. PRAS40 contains two proline-enriched stretches at the amino-

terminus and an Akt consensus phosphorylation site (RXRXXS/T) located at Thr246. Phosphorylated PRAS40 dissociates from mTORC1 resulting in mTORC activation in response to growth factors, insulin, glucose, and nutrients [39-41]. PRAS40 is expressed and regulated by Akt in cardiomyocytes (**Figure 4**). Furthermore, findings presented herein demonstrate that clinically relevant AAV-gene therapy with PRAS40 is protective in response to infarction injury. Importantly, PRAS40 overexpression reduced mortality after myocardial infarction and improved cardiac function (**Figure 6**). PRAS40 reduced ischemic injury in myocytes in part via increased mTORC2 signaling, since genetic interference with the PI3K-Akt-Rictor pathway resulted in loss of protection (**Figure 8**). Prevention of pathological remodeling with decreased fibrosis in the remote area and prevention of deregulations of sarcoplasmic reticulum calcium handling proteins likely contributes to improved contractile function after PRAS40 overexpression after MI. Overall, our findings concur with previous reports of PRAS40 involvement in regulation of Akt-dependent cell survival and apoptosis [42-44]. Importance of PRAS40/mTORC2 is also supported by recent reports that PRAS40 protects neurons from death after spinal cord injury [43,44]. In addition to regulation of mTOR kinase acivity, unbound PRAS40 may have additional effects in complexes formed with 14-3-3 and FoxO resulting in cytoplasmic retention of FoxO, downregulation of proapoptotic genes, and resistance to cell death [45].

Recent advancements in the development of AAV vectors have enabled the first clinical trial with AAV based cardiac specific gene transfer [46,47]. Thus, cardioprotection by PRAS40 could represent a future therapeutic option for treatment of myocardial injury. Traditional molecular interventions have focused upon inhibition of pathological remodeling and potentiation of cell survival or growth: two goals that are often at odds with one another. The unique capacity of PRAS40 to block hypertrophic growth while concurrently promoting

TORC2-mediated cell survival without impacting cardiac function represents a previously unrecognized constellation of features to prevent cardiac dysfunction. Correctly timed inhibition of mTORC1 in conjunction with mTORC2 potentiation could be a potent combinatorial approach to blunt cellular losses and ameliorate progression degenerative changes accompanying ischemic damage.

Acknowledgments: We would like to thank all members of the M.A.S laboratory for helpful discussion and comments.

Funding Sources: This study was supported by grants of the NIH to Mark Sussman and Christopher Glembotski , the Deutsche Forschungsgemeinschaft (1659/1-1 to Mirko Völkers and 3900/1-1 to Mathias Konstandin), The Rees-Stealy Research Foundation to Shabana Din, P.Q., and S.D. and the San Diego Chapter of the Achievement Rewards for College Scientists (ARCS) Foundation, the American Heart Association (Predoctoral Fellowship 10PRE3410005) and the Inamori Foundation to S.D..

Conflict of Interest Disclosures: None.

References:

1. Laplante M, Sabatini DM. mTOR Signaling in Growth Control and Disease. *Cell*. 2012;149:274–293.

2. Zoncu R, Efeyan A, Sabatini DM. mTOR: from growth signal integration to cancer, diabetes and ageing. *Nat Rev Mol Cell Biol*. 2010;12:21–35.

3. Sussman MA, Völkers M, Fischer K, Bailey B, Cottage CT, Din S, Gude N, Avitabile D, Alvarez R, Sundararaman B, Quijada P, Mason M, Konstandin MH, Malhowski A, Cheng Z, Khan M, McGregor M. Myocardial AKT: the omnipresent nexus. *Physiol. Rev.* 2011;91:1023–1070.

4. Zhang D, Contu R, Latronico MVG, Zhang JL, Rizzi R, Catalucci D, Miyamoto S, Huang K, Ceci M, Gu Y, Dalton ND, Peterson KL, Guan K-L, Brown JH, Chen J, Sonenberg N, Condorelli G. MTORC1 regulates cardiac function and myocyte survival through 4E-BP1 inhibition in mice. *J Clin Invest*. 2010;120:2805–2816.

5. McMullen JR. Inhibition of mTOR Signaling With Rapamycin Regresses Established Cardiac Hypertrophy Induced by Pressure Overload. *Circulation*. 2004;109:3050-3055.

6. Buss SJ, Muenz S, Riffel JH, Malekar P, Hagenmueller M, Weiss CS, Bea F, Bekeredjian R, Schinke-Braun M, Izumo S, Katus HA, Hardt SE. Beneficial Effects of Mammalian Target of Rapamycin Inhibition on Left Ventricular Remodeling After Myocardial Infarction. *J Am Coll Cardiol*. 2009;54:2435-2446.

7. Marin TM, Keith K, Davies B, Conner DA, Guha P, Kalaitzidis D, Wu X, Lauriol J, Wang B, Bauer M, Bronson R, Franchini KG, Neel BG, Kontaridis MI. Rapamycin reverses hypertrophic cardiomyopathy in a mouse model of LEOPARD syndrome–associated PTPN11 mutation. *J Clin Invest*. 2011;121:1026-1043.

8. Song X, Kusakari Y, Xiao CY, Kinsella SD, Rosenberg MA, Scherrer-Crosbie M, Hara K, Rosenzweig A, Matsui T. mTOR attenuates the inflammatory response in cardiomyocytes and prevents cardiac dysfunction in pathological hypertrophy. *AJP: Cell Physiology*. 2010;299:C1256-C1266.

9. Aoyagi T, Kusakari Y, Xiao C-Y, Inouye BT, Takahashi M, Scherrer-Crosbie M, Rosenzweig A, Hara K, Matsui T. Cardiac mTOR protects the heart against ischemia-reperfusion injury. *Am J Physiol Heart Circ Physiol*. 2012;303:H75-85.

10. Sarbassov DD, Ali SM, Sengupta S, Sheen J-H, Hsu PP, Bagley AF, Markhard AL, Sabatini DM. Prolonged Rapamycin Treatment Inhibits mTORC2 Assembly and Akt/PKB. *Mol Cell*. 2006;22:159-168.

11. Harston RK, McKillop JC, Moschella PC, Van Laer A, Quinones LS, Baicu CF, Balasubramanian S, Zile MR, Kuppuswamy D. Rapamycin treatment augments both protein ubiquitination and Akt activation in pressure-overloaded rat myocardium. *Am J Physiol Heart Circ Physiol*.. 2011;300:H1696-H1706.

12. Kuzman JA, O'Connell TD, Gerdes AM. Rapamycin Prevents Thyroid Hormone-Induced Cardiac Hypertrophy. *Endocrinology*. 2007;148:3477-3484.

13. Soesanto W, Lin HY, Hu E, Lefler S, Litwin SE, Sena S, Abel ED, Symons JD, Jalili T. Mammalian target of rapamycin is a critical regulator of cardiac hypertrophy in spontaneously hypertensive rats. *Hypertension*. 2009;54:1321-1327.

14. Huo Y, Iadevaia V, Proud CG. Differing effects of rapamycin and mTOR kinase inhibitors on protein synthesis. *Biochem Soc Trans*. 2011;39:446-450.

15. Oh WJ, Jacinto E. mTOR complex 2 signaling and functions. *Cell Cycle*. 2011;10:2305-2316.

16. Goncharova EA, Goncharov DA, Li H, Pimtong W, Lu S, Khavin I, Krymskaya VP. mTORC2 is required for proliferation and survival of TSC2-null cells. *Mol Cell Biol*.

2011;31:2484-2498.

17. Sasaki T, Irie-Sasaki J, Jones RG, Oliveira-dos-Santos AJ, Stanford WL, Bolon B, Wakeham A, Itie A, Bouchard D, Kozieradzki I, Joza N, Mak TW, Ohashi PS, Suzuki A, Penninger JM. Function of PI3Kgamma in thymocyte development, T cell activation, and neutrophil migration. *Science*. 2000;287:1040-1046.

18. Muraski JA, Rota M, Misao Y, Fransioli J, Cottage C, Gude N, Esposito G, Delucchi F, Arcarese M, Alvarez R, Siddiqi S, Emmanuel GN, Wu W, Fischer K, Martindale JJ, Glembotski CC, Leri A, Kajstura J, Magnuson N, Berns A, Beretta RM, Houser SR, Schaefer EM, Anversa P, Sussman MA. Pim-1 regulates cardiomyocyte survival downstream of Akt. *Nat Med.* 2007;13:1467-1475.

19. Quijada P, Toko H, Fischer KM, Bailey B, Reilly P, Hunt KD, Gude NA, Avitabile D, Sussman MA. Preservation of myocardial structure is enhanced by pim-1 engineering of bone marrow cells. *Circ Res*. 2012;111:77-86.

20. Cheng Z, Völkers M, Din S, Avitabile D, Khan M, Gude N, Mohsin S, Bo T, Truffa S, Alvarez R, Mason M, Fischer KM, Konstandin MH, Zhang X-K, Heller Brown J, Sussman MA. Mitochondrial translocation of Nur77 mediates cardiomyocyte apoptosis. *Eur Heart J.* 2011;32:2179-2188.

21. Völkers M, Weidenhammer C, Herzog N, Qiu G, Spaich K, Wegner von F, Peppel K, Müller OJ, Schinkel S, Rabinowitz JE, Hippe H-J, Brinks H, Katus HA, Koch WJ, Eckhart AD, Friedrich O, Most P. The inotropic peptide βARKct improves βAR responsiveness in normal and failing cardiomyocytes through G(βγ)-mediated L-type calcium current disinhibition. *Circ Res*. 2011;108:27-39.

22. Avitabile D, Bailey B, Cottage CT, Sundararaman B, Joyo A, McGregor M, Gude N, Truffa S, Zarrabi A, Konstandin M, Khan M, Mohsin S, Völkers M, Toko H, Mason M, Cheng Z, Din S, Alvarez R, Fischer K, Sussman MA. Nucleolar stress is an early response to myocardial damage involving nucleolar proteins nucleostemin and nucleophosmin. *Proc Natl Acad Sci U S A*. 2011;108:6145-6150.

23. Liu Q, Chang JW, Wang J, Kang SA, Thoreen CC, Markhard A, Hur W, Zhang J, Sim T, Sabatini DM, Gray NS. Discovery of 1-(4-(4-Propionylpiperazin-1-yl)-3-(trifluoromethyl)phenyl)-9-(quinolin-3-yl)benzo[h][1,6]naphthyridin-2(1 H)-one as a Highly Potent, Selective Mammalian Target of Rapamycin (mTOR) Inhibitor for the Treatment of Cancer. *J. Med. Chem.* 2010;53:7146-7155.

24. Shende P, Plaisance I, Morandi C, Pellieux C, Berthonneche C, Zorzato F, Krishnan J, Lerch R, Hall MN, Ruegg MA, Pedrazzini T, Brink M. Cardiac Raptor Ablation Impairs Adaptive Hypertrophy, Alters Metabolic Gene Expression, and Causes Heart Failure in Mice. *Circulation*. 2011;123:1073-1082.

25. Guertin DA, Stevens DM, Thoreen CC, Burds AA, Kalaany NY, Moffat J, Brown M,

Fitzgerald KJ, Sabatini DM. Ablation in mice of the mTORC components raptor, rictor, or mLST8 reveals that mTORC2 is required for signaling to Akt-FOXO and PKCalpha, but not S6K1. *Developmental Cell*. 2006;11:859-871.

26. Sancak Y, Thoreen CC, Peterson TR, Lindquist RA, Kang SA, Spooner E, Carr SA, Sabatini DM. PRAS40 is an insulin-regulated inhibitor of the mTORC1 protein kinase. *Mol Cell*. 2007;25:903-915.

27. Vander Haar E, Lee SI, Bandhakavi S, Griffin TJ, Kim DH. Insulin signalling to mTOR mediated by the Akt/PKB substrate PRAS40. *Nat Cell Biol*. 2007;9:316-323.

28. Siragusa M, Katare R, Meloni M, Damilano F, Hirsch E, Emanueli C, Madeddu P. Involvement of Phosphoinositide 3-Kinase in Angiogenesis and Healing of Experimental Myocardial Infarction in Mice. *Circ Res*. 2010;106:75-768.

29. Hung C-M, Garcia-Haro L, Sparks CA, Guertin DA. mTOR-dependent cell survival mechanisms. *Cold Spring Harb Perspect Biol*. 2012;4.

30. Koitabashi N, Kass DA. Reverse remodeling in heart failure—mechanisms and therapeutic opportunities. *Nat Rev Cardiol*. 2011;9:147-157.

31. McKinsey TA, Kass DA. Small-molecule therapies for cardiac hypertrophy: moving beneath the cell surface. *Nat Rev Drug Discov*. 2007;6:617-635.

32. Sciarretta S, Zhai P, Shao D, Maejima Y, Robbins J, Volpe M, Condorelli G, Sadoshima J. Rheb is a Critical Regulator of Autophagy During Myocardial Ischemia: Pathophysiological Implications in Obesity and Metabolic Syndrome. *Circulation*. 2012;125:1134-1146.

33. Wander SA, Hennessy BT, Slingerland JM. Next-generation mTOR inhibitors in clinical oncology: how pathway complexity informs therapeutic strategy. *J Clin Invest*. 2011;121:1231-1241.

34. Hagiwara A, Cornu M, Cybulski N, Polak P, Betz C, Trapani F, Terracciano L, Heim MH, Rüegg MA, Hall MN. Hepatic mTORC2 Activates Glycolysis and Lipogenesis through Akt, Glucokinase, and SREBP1c. *Cell Metab*. 2012;15:725-738.

35. Wang R-H, Kim H-S, Xiao C, Xu X, Gavrilova O, Deng C-X. Hepatic Sirt1 deficiency in mice impairs mTorc2/Akt signaling and results in hyperglycemia, oxidative damage, and insulin resistance. *J Clin Invest*. 2011;121:4477-4490.

36. Zhang X, Tang N, Hadden TJ, Rishi AK. Akt, FoxO and regulation of apoptosis. *Biochim Biophys Acta*. 2011;1813:1978-1986.

37. Ronnebaum SM, Patterson C. The FoxO Family in Cardiac Function and Dysfunction. *Annu Rev Physiol*. 2010;72:81-94.

38. Kovacina KS, Park GY, Bae SS, Guzzetta AW, Schaefer E, Birnbaum MJ, Roth RA. Identification of a proline-rich Akt substrate as a 14-3-3 binding partner. *J Biol Chem*. 2003;278:10189-10194.

39. Oshiro N, Takahashi R, Yoshino K-I, Tanimura K, Nakashima A, Eguchi S, Miyamoto T, Hara K, Takehana K, Avruch J, Kikkawa U, Yonezawa K. The proline-rich Akt substrate of 40 kDa (PRAS40) is a physiological substrate of mammalian target of rapamycin complex 1. *J Biol Chem*. 2007;282:20329-20339.

40. Wiza C, Nascimento EBM, Ouwens DM. Role of PRAS40 in Akt and mTOR signaling in health and disease. *Am J Pathol.* 2012;302:E1453-1460.

41. Fonseca BD, Smith EM, Lee VH, Mackintosh C, Proud CG. PRAS40 is a target for mammalian target of rapamycin complex 1 and is required for signaling downstream of this complex. *J Biol Chem.* 2007;282:24514-24524.

42. Saito A, Hayashi T, Okuno S, Nishi T, Chan PH. Modulation of proline-rich akt substrate survival signaling pathways by oxidative stress in mouse brains after transient focal cerebral ischemia. *Stroke*. 2006;37:513-517.

43. Saito A, Narasimhan P, Hayashi T, Okuno S, Ferrand-Drake M, Chan PH. Neuroprotective role of a proline-rich Akt substrate in apoptotic neuronal cell death after stroke: relationships with nerve growth factor. *J Neurosci*. 2004;24:1584-1593.

44. Yu F, Narasimhan P, Saito A, Liu J, Chan PH. Increased expression of a proline-rich Akt substrate (PRAS40) in human copper/zinc-superoxide dismutase transgenic rats protects motor neurons from death after spinal cord injury. *J Cereb Blood Flow Metab*. 2008;28:44-52.

45. Kim W, Youn H, Seong KM, Yang HJ, Yun YJ, Kwon T, Kim YH, Lee JY, Jin Y-W, Youn B. PIM1-activated PRAS40 regulates radioresistance in non-small cell lung cancer cells through interplay with FOXO3a, 14-3-3 and protein phosphatases. *Radiat Res.* 2011;176:539-552.

46. Pacak CA, Byrne BJ. AAV Vectors for Cardiac Gene Transfer: Experimental Tools and Clinical Opportunities. *Mol Ther*. 2009;19:1582-1590.

47. Jaski BE, Jessup ML, Mancini DM, Cappola TP, Pauly DF, Greenberg B, Borow K, Dittrich H, Zsebo KM, Hajjar RJ, Calcium Up-Regulation by Percutaneous Administration of Gene Therapy In Cardiac Disease (CUPID) Trial Investigators. Calcium upregulation by percutaneous administration of gene therapy in cardiac disease (CUPID Trial), a first-in-human phase 1/2 clinical trial. *J Card Fail.* 2009;15:171-181.

DOI: 10.1161/CIRCULATIONAHA.113.003638

Figure Legends:

Figure 1. Decreasing mTORC1 and mTORC2 activity increases damage after stress. **(A)** Schematic overview of mTOR signaling. **(B)** mTORC1 and mTORC2 are inactivated after treatment with Torin1 as shown by immunoblots. **(C)** Cell death in NRCMs. Challenge with H_2O_2 (50μM for 4h) after mTOR kinase inhibition with Torin1 (50nM). Torin1 exposure increases apoptosis in response to H_2O_2. *p<0.05 versus Veh, #p<0.05 versus Veh H_20_2 Veh. **(D)** Torin1 inhibits mTOR kinase activity *in vivo* as shown by immunoblots. **(E)** Kaplan-Meier survival curve of vehicle and Torin1 (5mg/kg BW) injected mice. Mortality early after infarction is increased after injection of Torin1. n=4 in the sham groups. **(F)** Torin1 increases infarct size. p<0.05 vs control MI. **(G)** Representative confocal scans are shown for TUNEL, actin, and nuclei (red, green and blue, respectively, in overlays). Bar=150μm. Percentage of TUNEL-labeled cells in the left ventricle of remote area 1 day after MI. *p<0.05 vs control MI. **(H)** Echocardiographic assessment of control or Torin1 injected mice for EF and left ventricular end-diastolic volume (EDV). *p<0.05 versus Sham, #p<0.05 versus Mi Veh. Hemodynamic measurements of ±dP/dT 2 weeks post-surgery. *p<0.05 versus Sham, #p<0.05 versus Mi Veh. Numbers of mice or number of independent experiments per group are indicated in the bar graphs.

Figure 2. Loss of mTORC2 signaling increases cardiomyocyte death *in vitro*. **(A)** Silencing of Raptor confirmed by immunoblot. (**B)** Barplots depicting quantitation of Akt phosphorylation, RibS6 phosphorylation after Raptor silencing. *p<0.05 versus Scr, #p<0.05 versus Scr H_20_2 Veh **(C)** Barplots depicting quantitation of Rictor, mTOR and Raptor expression after Raptor silencing. n=4 independent experiments. **(D)** Cell death in NRCMs. Rictor silencing but not

Raptor silencing increases cell death after challenge with H_2O_2 (50μM for 4h). *p<0.05 versus Control, #*p<0.05 versus Scr H_2O_2. n=5 independent experiments **(E)** Silencing of Rictor confirmed by immunoblot. n=4 independent experiments **(F)** Barplots depicting quantitation of Akt phosphorylation, RibS6 phosphorylation after Rictor silencing. *p<0.05 versus Scr, #p<0.05 versus Scr H_20_2 Veh. n=4 independent experiments **(G)** Histogram depicting quantitation of Raptor, mTOR and Rictor expression after Rictor silencing. n=4 independent experiments

Figure 3. Loss of mTORC2 signaling increases cardiomyocyte damage after MI. **(A)** Silencing of Rictor confirmed by immunoblot. AAV-sh-Rictor hearts exhibit decreased Akt phosphorylation without altered mTORC1 activation. **(B)** Barplots depicting quantitation of Raptor/mTOR/Rictor expression. *p<0.05 versus control Sham. n=3 per group **(C)** Barplots depicting quantitation of pRibS6 phosphorylation. n=3 per group **(D)** Kaplan-Meier survival curve of AAV-sh-Control and AAV-sh-Rictor mice. AAV-sh-Rictor increases mortality early after infarction. n=6 in the sham groups. **(E)** Percentage of TUNEL-labeled cells in the left ventricle of the remote area 1 day after MI..*p<0.05 vs control MI. **(F)** Echocardiographic assessment of AAV-sh-Control or AAV-sh-Rictor mice for ejection fraction (EF) and left ventricular end-diastolic volume (LVEDV). *p<0.05 versus shcontrol Sham, #p<0.05 versus MI shControl. (**G)** Silencing of Rictor in myocytes confirmed by confocal microscopy. Representative confocal scans for Rictor, actin and nuclei (green, red and blue, respectively, in overlays. interstitial non-myocytes express Rictor in AAV-sh-Rictor hearts (arrow) Bar=150μm. (**H)** Masson-Trichrome staining from control and shRictor treated hearts. Barplots depicting quantifaction of fibrotic area. *p<0.05 versus control Sham. #p<0.05 versus MI.. Bar=1mm. Numbers of mice per group are indicated in the bar graphs.

Figure 4. mTORC2 function is necessary for PRAS40 mediated protection**. (A)** Cell death quantified by flow cytometric detection upon H_2O_2 treatment.. Torin1 blunts protective effects of PRAS40. *p<0.05 compared to control. $p<0.05 compared to control H_2O_2 **(B)** mTOR kinase inhibition after Torin1 (50nM) confirmed by immunoblot. **(C)** siRNA Akt silencing blunts PRAS40 induced protection. Data depicted as percentage dead cells. ***p<0.001 compared to control. #:p<0.05 compared to control H_2O_2 **(D)** Akt1 silencing confirmed by immunoblot. **(E)** siRNA Rictor silencing, but not Raptor silencing blunts PRA40 induced protection. Data depicted as percentage dead cells.. ***p<0.001 compared to control. #:p<0.05 compared to control H_2O_2. $$p<0.01 vs control H_2O_2. **(F)** Rictor or Raptor silencing and blunting of mTOR downstream target phosphorylation by immunoblot. Numbers of independent experiments per group are indicated in the bar graphs.

Figure 5. PRAS40 protects against ischemic injury**. (A)** Kaplan–Meier survival analysis of control and PRAS40 animals following MI or sham operation. Masson-Trichrome staining of control and PRAS40 treated hearts 6 weeks after surgery. n=5 for the Sham groups. **(B)** Infarct size measurements 6 weeks after MI. *P<0.05 versus control MI. **(C)** Percentage of TUNEL-labeled myocytes in the left ventricle in the remote area 2d after MI. *p<0.05 vs control MI. **(D)** Weekly echocardiographic assessment of control or PRAS40 sham and MI hearts for EF and left ventricular end-diastolic volume (LVEDV). *p<0.05 versus control MI, n=14-15 for the MI group and n=5-6 for Sham. **(E)** In vivo hemodynamic measurements of ±dP/dT and left ventricular end-diastolic pressure (LVEDP) 6 weeks post-surgery. **(F)** HW/BW in control and PRAS40 mice 6 weeks after sham and MI surgery. **(G)** Cardiomyocyte area (CSA) in control and PRAS40 mice 6 weeks after sham or MI surgery (*p< 0.01 versus control sham; #p< 0.05 versus

control MI. **(H)** Nppa and Nppb transcription in hearts of mice of the indicated group 6 weeks after Sham or MI (*p<0.01 versus Control sham; #p<0.05 versus Control MI). Error bars indicate means ± sem. (**I)** Masson-Trichrome staining from control and PRAS40 treated hearts. Barplots depicting quantifaction of fibrotic area. *p<0.05 versus control Sham. #p<0.05 versus MI.. Bar=1mm **(J)** Collagen1 transcription in hearts of mice of the indicated group 6 weeks after Sham or MI (*p<0.01 versus Control sham; #p<0.05 versus Control MI). Error bars indicate means ± sem. Number of mice per group is indicated within the bar.

Figure 6. PRAS40 promotes protective mTORC2 signaling in vivo**. (A)** Heart lysates for indicated proteins 2d after MI assessed by immunoblot. Akt phosphorylation quantitation histogram. p<0.01 versus Control sham; #p<0.05 versus Control MI). **(B)** Heart lysates for indicated proteins 2d after MI assessed by immunoblot. RibS6 phosphorylation quantiation by histogram. (*p<0.01 versus Control sham; #p<0.05 versus Control MI). **(C)** Paraffin-embedded sections from control hearts and PRAS40 treated hearts 2d after MI stained for $pAkt^{473}$ (red), actin (green) and nuclei (blue) assessed by confocal microscopy. **(D)** Sections of control hearts and PRAS40 treated hearts 2d after MI stained for pRibS6 (red), actin (green) and nuclei (blue) assessed by confocal microscopy. Bar=150μm. **(E)** Heart lysates assessed for indicated protein expression 6 weeks after surgery by immunoblot. **(F)** PRAS40 overexpression increases of Akt phosphorylation in myocytes by confocal microscopy of myocardial sections at 6 weeks post surgery. Bar=50μm. Number of mice per group is indicated within the bar.

Figure 7. Cardioprotection by PRAS40 is mTORC2 dependent in vivo. **(A)** Ejection fraction (EF) and left ventricular end diastolic volume (LVEDV) in $PI3K^{-/-}$ mice before and after MI

assessed by echocardiography. **(B)** EF and LVEDV in Akt1$^{-/-}$ mice before and after MI assessed by echocardiography. **(C)** EF and LVEDV in mice injected with AAV-sh-Control, AAV-sh-Rictor, AAV-PRAS40 or AAV-sh-Rictor and AAV-PRAS40 assessed by echocardiography. *p<0.05 compared to shControl. #:p<0.05 compared to shControl **(D)** HW/BW in mice 2 weeks after MI surgery. *p<0.05 compared to shControl **(E)** Percentage of TUNEL-labeled myocytes in the left ventricle in the remote area 1d after MI. n=3 per group, *p<0.05 vs control MI, #p<0.05 compared to shControl. Bar=150μm. Number of mice per group is indicated within the bar.

Figure 8. Model for PRAS40 mediated cardioprotection. mTOR kinase inhibitors or impairment of mTORC2 function worsens cardiac function after myocardial infarction. PRAS40 blocks mTORC1 in myocytes and diverts toward mTORC2 function, increasing Akt activation leading to increased cellular survival after infarction.

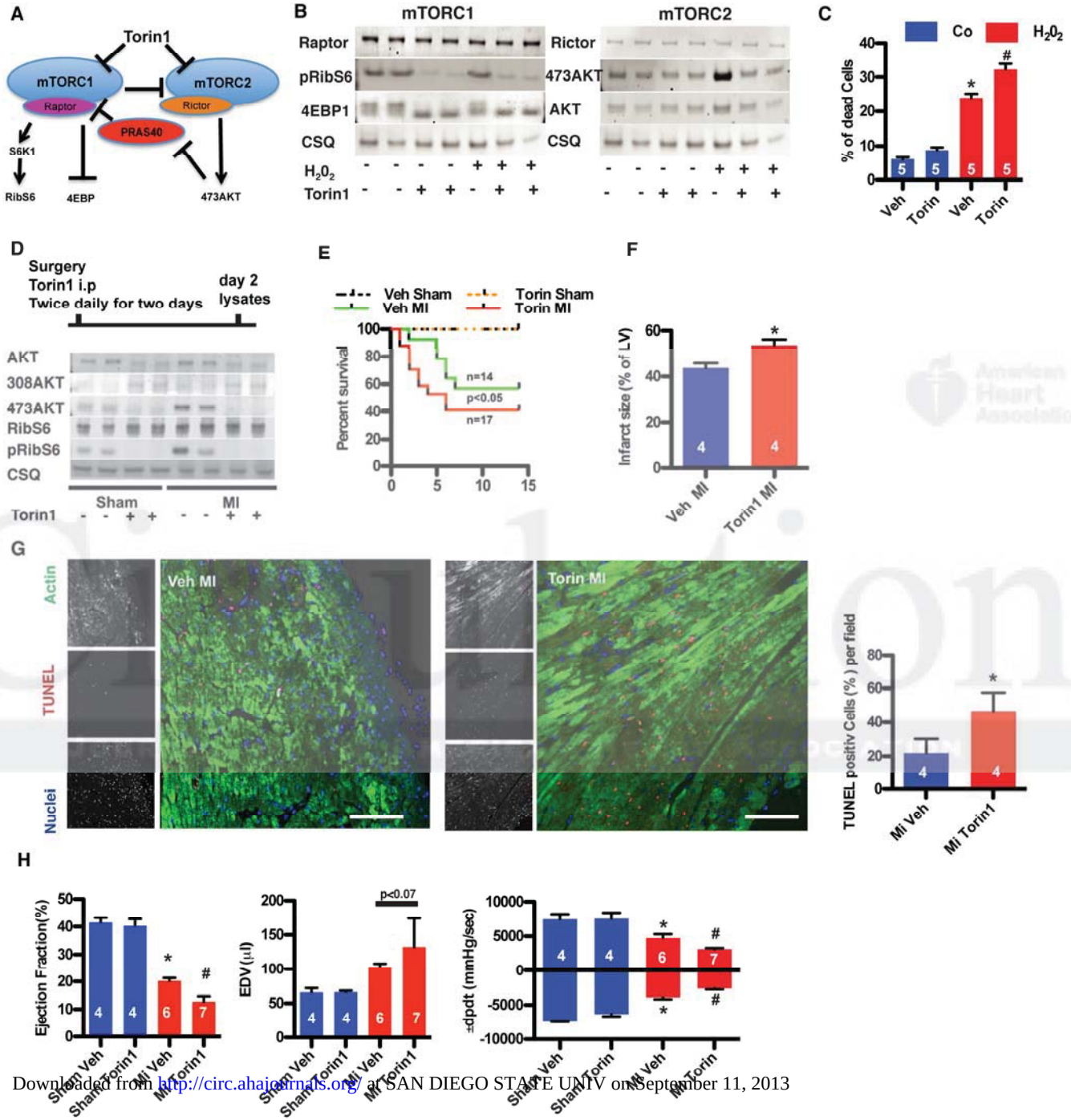

Figure 1

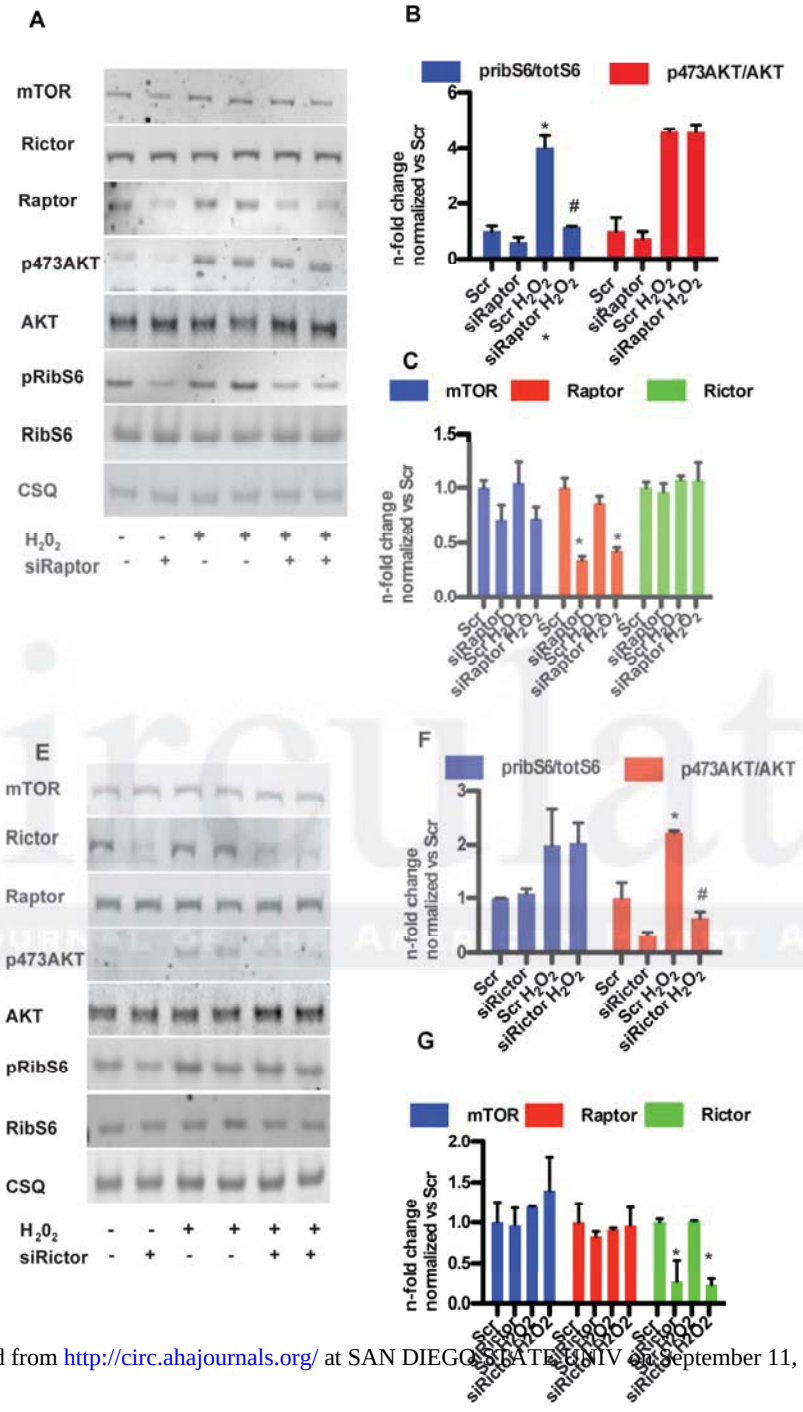

Figure 2

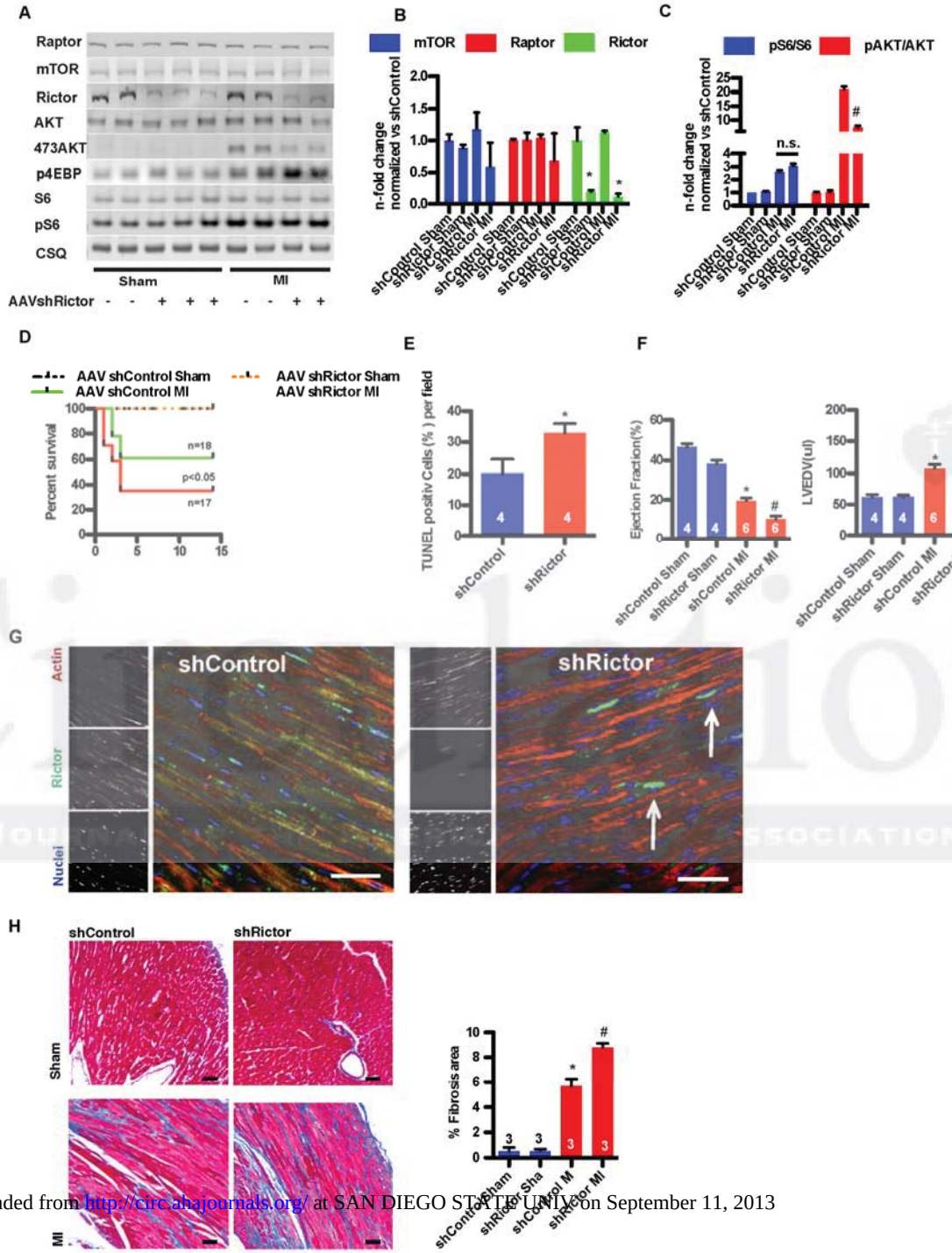

Figure 3

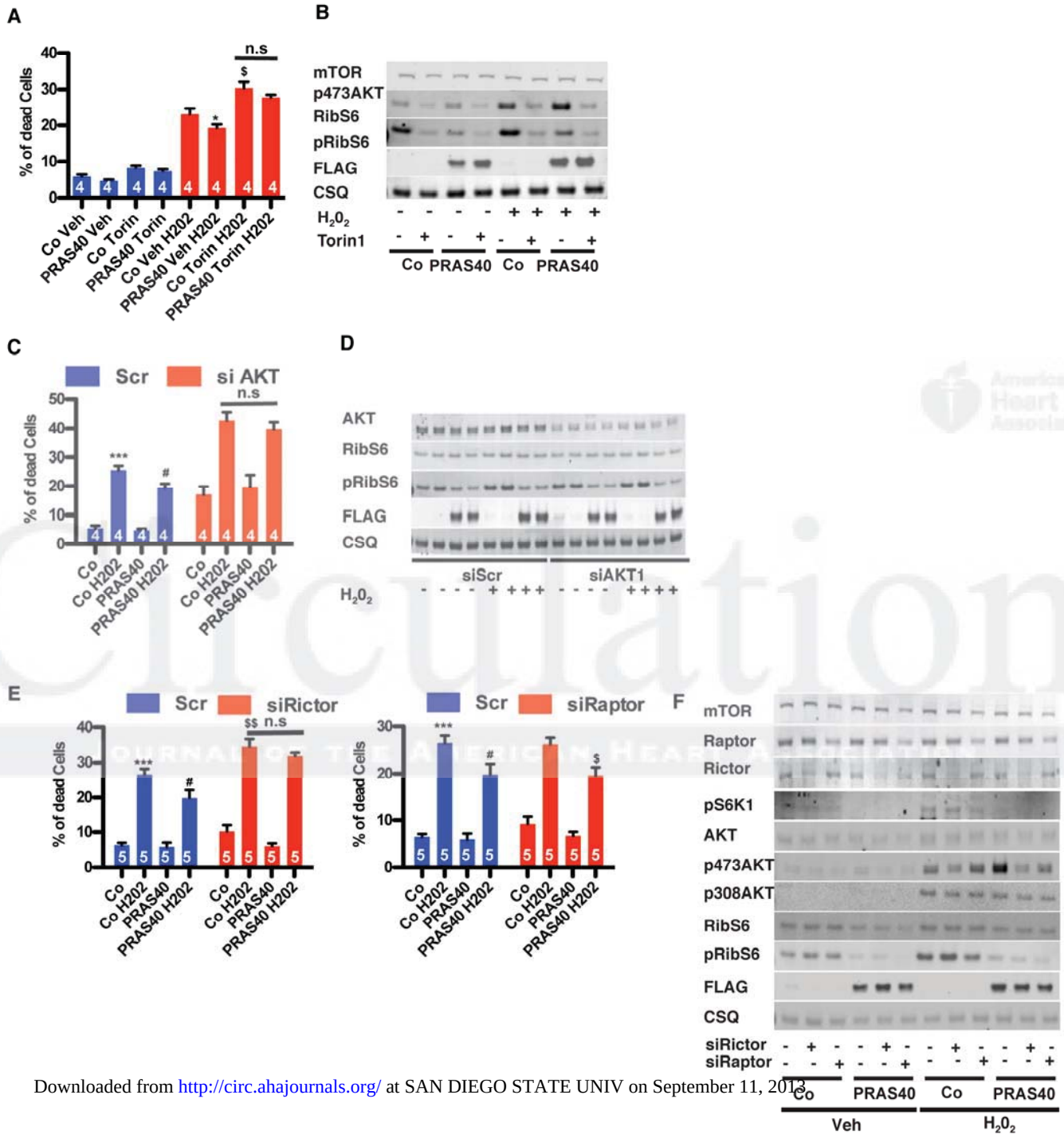

Figure 4

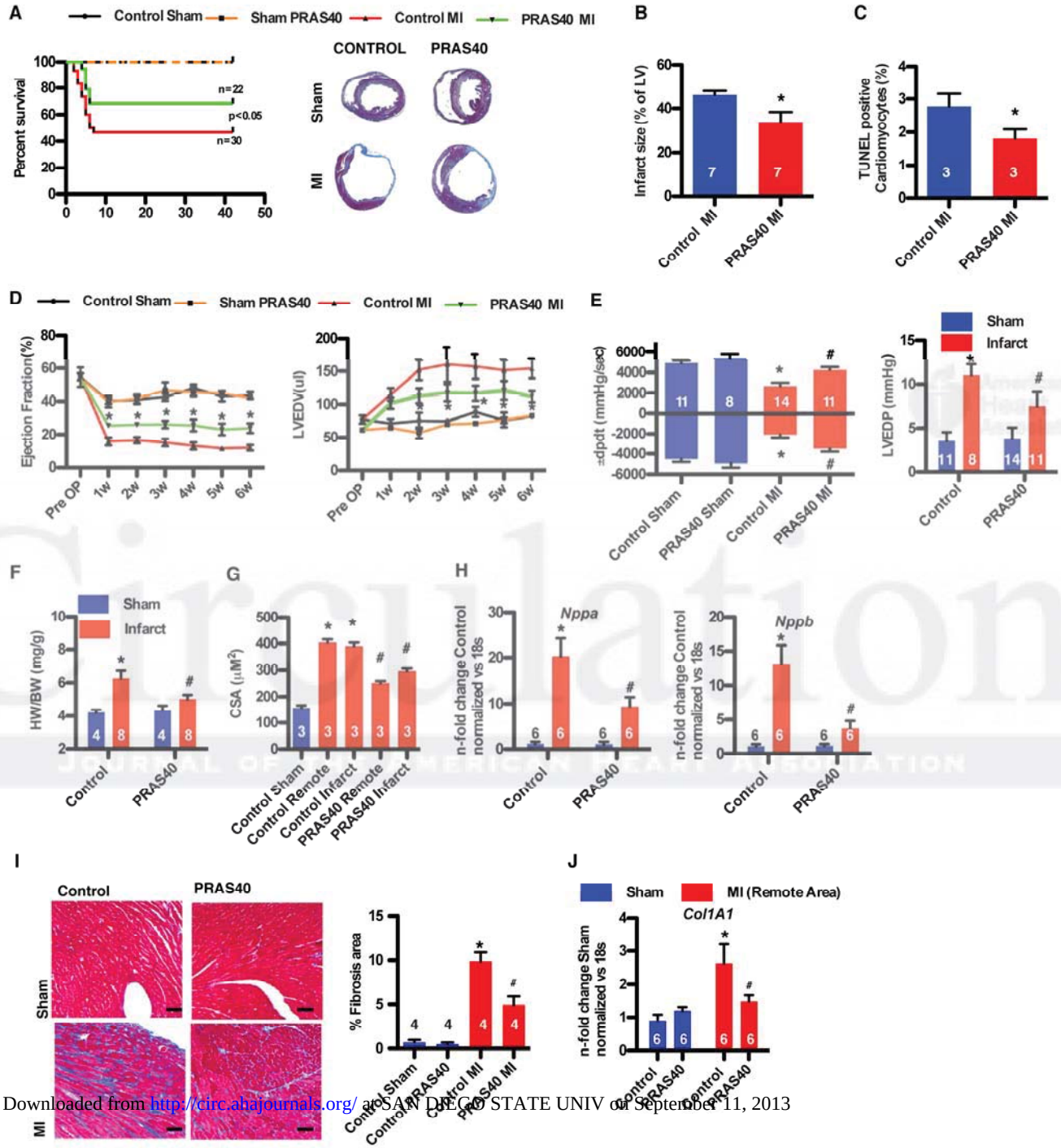

Figure 5

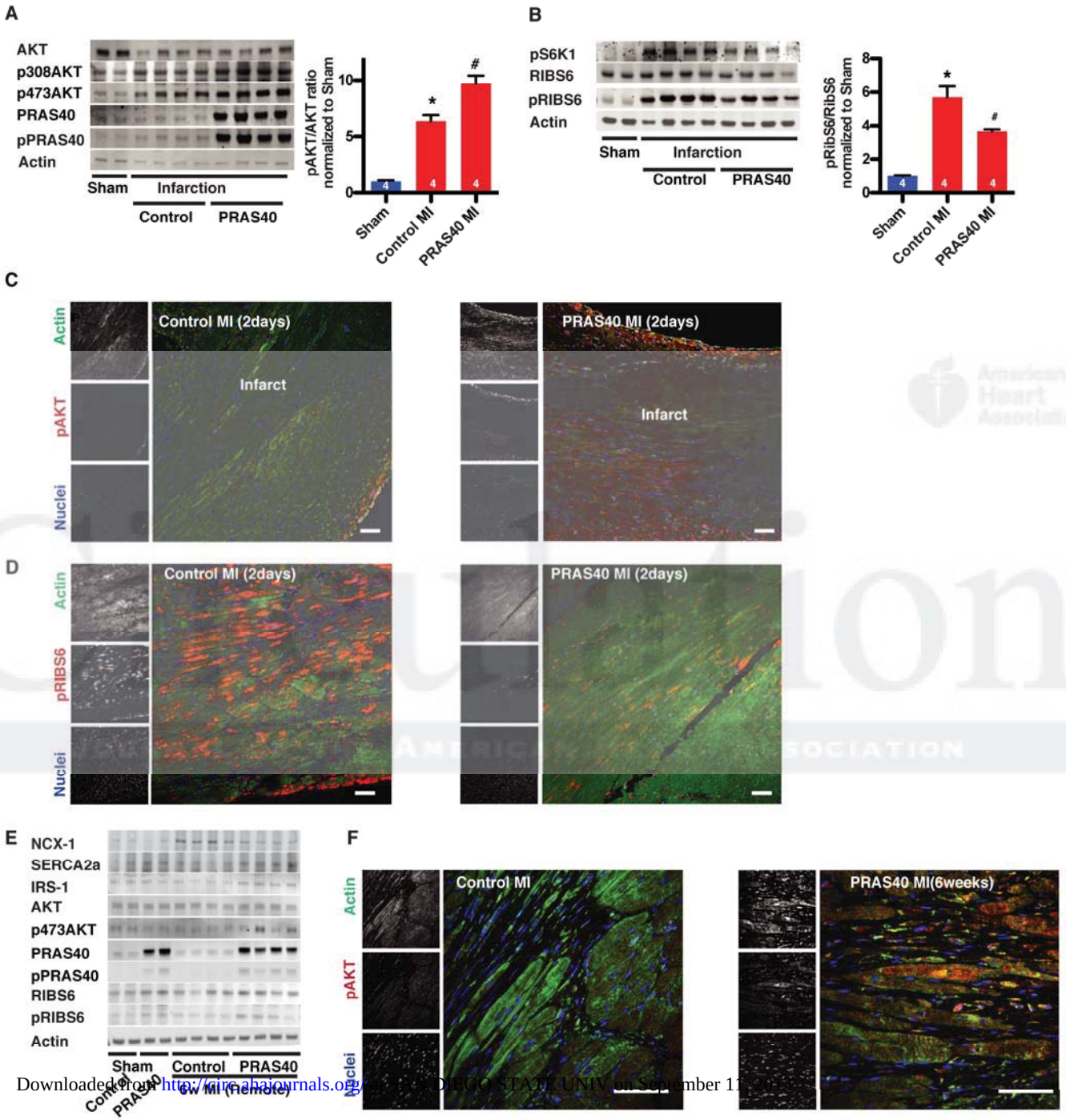

Figure 6

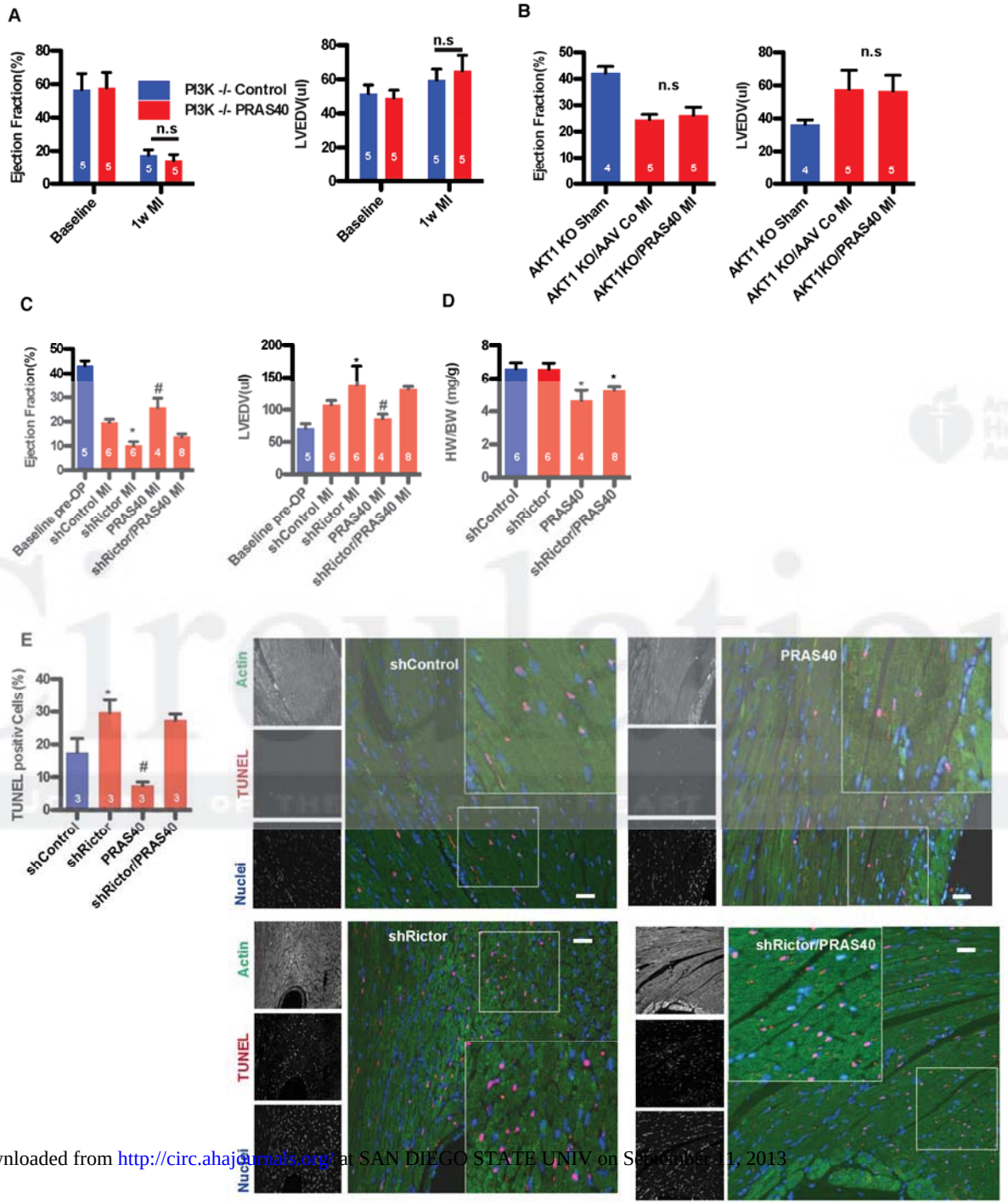

Figure 7

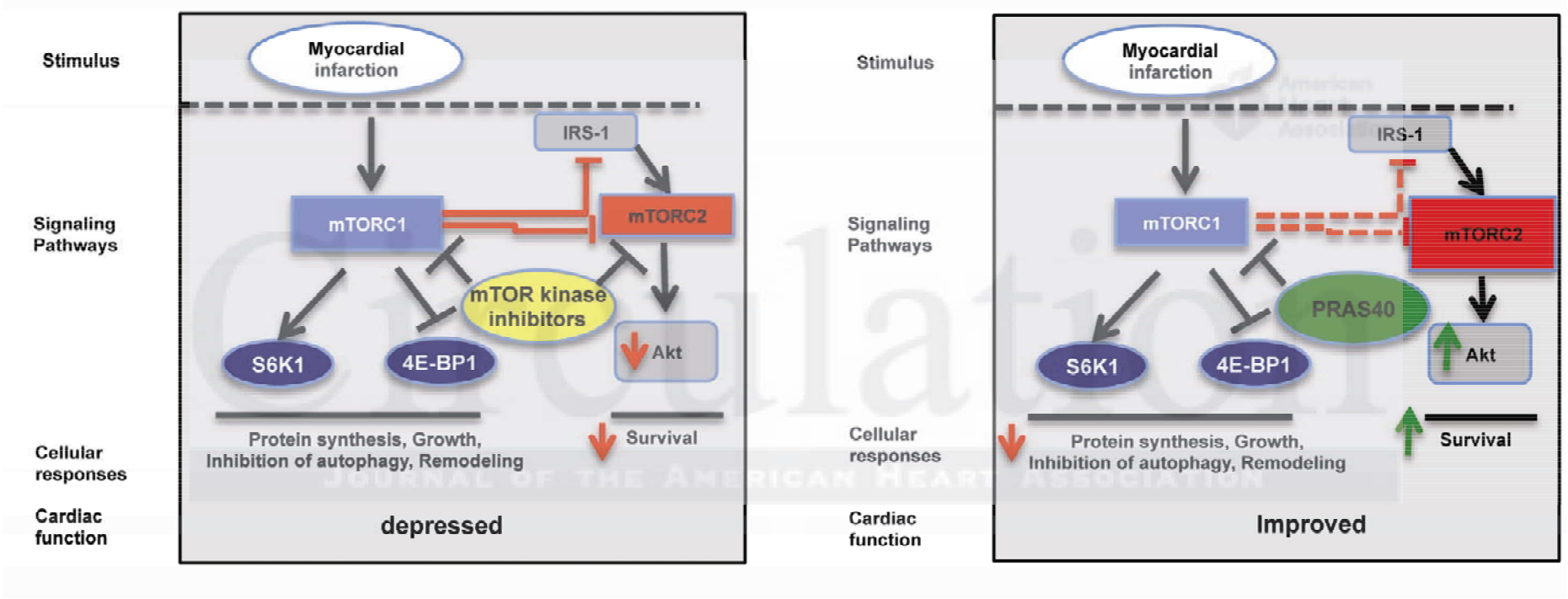

Figure 8